IEEE Access
Multidisciplinary ⋮ Rapid Review ⋮ Open Access Journal

Received 6 November 2024, accepted 22 November 2024, date of publication 27 November 2024,
date of current version 9 December 2024.

Digital Object Identifier 10.1109/ACCESS.2024.3507367

RESEARCH ARTICLE

Reduced Order Modeling for Thermal Simulations of Electric Components With Surface-to-Surface Radiation

MATTEO ZORZETTO[1], RICCARDO TORCHIO[1,2], FRANCESCO LUCCHINI[1], STEFANO MASSEI[3], LEONARDO ROBOL[3], AND FABRIZIO DUGHIERO[1]

[1]Department of Industrial Engineering, Università degli Studi di Padova, 35131 Padua, Italy
[2]Department of Information Engineering, Università degli Studi di Padova, 35131 Padua, Italy
[3]Department of Mathematics, University of Pisa, 56127 Pisa, Italy

Corresponding author: Riccardo Torchio (riccardo.torchio@unipd.it)

The work of Stefano Massei was supported by the Ministero dell'istruzione, dell'università e della ricerca (MIUR) Excellence Department Project awarded to the Department of Mathematics, University of Pisa, under Grant CUP I57G22000700001. The work of Leonardo Robol was supported in part by the National Research Center in High Performance Computing, Big Data and Quantum Computing, under Grant CN1–Spoke 6; and in part by the MIUR Excellence Department Project awarded by the Department of Mathematics, University of Pisa, under Grant CUP I57G22000700001.

ABSTRACT This paper introduces the application of a reduced-order modeling technique for accurate temperature monitoring in Power Electronics modules. The methodology involves coupling the Finite Element Method with the radiosity equation to obtain a high-fidelity representation of the physical behavior of the device. These models account also for surface-to-surface radiation, an aspect that can have a high impact when the operating temperatures increase, and the components are close to each other, which is a common scenario for high power density and compact modules. The Model Order Reduction is performed via the Proper orthogonal decomposition, coupled with the Discrete Empirical Interpolation Method to handle the nonlinearity introduced by the surface-to-surface radiation. This approach allows to reduce the computation time with a limited effect on the accuracy of the prediction. The method is applied to reduce the order of the thermal model of a DC-DC converter. Numerical and experimental results demonstrate the approach's effectiveness, showcasing high accuracy with minimal computation time and memory cost.

INDEX TERMS Discrete empirical interpolation method (DEIM), finite element method (FEM), model order reduction (MOR), radiative heat transfer.

I. INTRODUCTION

The increase in power density, along with the desire to have small-sized components, has led to increased compactness of Power Electronics (PE) modules. This means that several devices, some among them emitting heat, are near each other, typically within an enclosure. In PE converters, compactness is often achieved by increasing the switching frequency, thus reducing the dimensions of the passive components [1], and by packing them in close proximity [2]. Small-sized modules, with high power density (like the one seen in Fig. 1), require a high power heat dissipation, which may lead to dangerous hot spots [3], [4]. High operating temperatures and switching frequencies are typical of power modules made with wide-band-gap semiconductors like silicon carbide (SiC) [5], [6]. Developing thermal models for these high-power converters is crucial, given their application across various renewable technologies. These include electric vehicles and trains, as well as inverters for photovoltaic (PV) systems [7].

Indeed, having an accurate thermal model is important during the design and optimization of such components, where several time-consuming simulations must be done to check the reliability of the analyzed design, as the temperature is one of the main causes of failure in electronics [8].

Furthermore, accurate thermal models for PE components are crucial when implementing advanced control strategies, such as those rooted in Model Predictive Control (MPC) techniques [9]. These models can serve as soft sensors, providing virtual measurements of quantities that are challenging to probe [10], [11]. In this scenario, a computationally light

The associate editor coordinating the review of this manuscript and approving it for publication was Su Yan.

model is desired, since real-time (or faster than real-time) simulations of the model are required [12].

When developing such models, the impact of thermal radiation is frequently disregarded due to its introduction of non-linearity, which consequently renders the problem more complex and challenging to resolve. This omission is justified when operating temperatures remain low since the portion of heat dissipated through radiation is insignificant compared to conduction and convection [13]. However, this is not the case for, e.g., high power density and compact module applications, where the operating temperature is high. For example, in an enclosure, heat dissipates from the component primarily through conduction and thermal radiation [14]. This is particularly true when airflow is restricted, hindering natural convection and thus making it ineffective for efficient device cooling [15]. In [14], Dallago and Venchi performed thermal simulations of a notebook that employed a fully passive thermal solution. When simulating the model without accounting for thermal radiation, the temperature of some components increased up to 56% [14].

It is noteworthy that, when radiation is considered, two phenomena exist: surface-to-ambient (s2a) radiation, where the components exchange heat by radiation toward the surrounding ambient with a presumed constant temperature, and surface-to-surface (s2s) radiation, where different parts of the components at different temperatures mutually exchange heat [16]. This latter phenomenon contributes to the heating of components placed in proximity to heat-dissipating ones. Usually, because of their simplicity, thermal networks are adopted to model PE components. However, in general, thermal networks only allow for low-resolution temperature monitoring [3], [17].

More accurate thermal models of electric components can be obtained by using the finite element method (FEM), which transforms the heat conduction problem into a large system of equations. Coupling the FEM with thermal radiation provides an accurate but computationally expensive representation of the phenomena. In particular, including s2a thermal radiation makes the problem non-linear, and including s2s radiation requires generating, storing, and operating with dense matrices representing the non-local heat exchange between different parts of the component, thus significantly increasing the computational burden of the model [18], [19].

Projection-based Model Order Reduction (MOR) techniques aim to simplify a Full Order Model (FOM) by projecting its system matrices onto a lower-dimensional subspace. This process results in a Reduced Order Model (ROM), which retains the essential dynamics of the original system while substantially reducing computation time and memory requirements, with only a limited loss of accuracy. Various MOR techniques can be employed to determine the appropriate reduced basis for projecting the FOM. For instance, techniques employing Krylov spaces methods, such as ones based on the Lanczos and Arnoldi algorithms [20], [21], [22], [23], derive the reduced basis by matching the system's response. Alternatively, Balanced Truncation (BT) works by "balancing" the system, i.e. making it equally observable and controllable, before truncating the less significant modes [20]. While BT offers an a priori error estimate, its computational complexity can become prohibitive, primarily due to the need to solve Lyapunov matrix equations. This can be addressed using low-rank solvers for linear matrix equations [24], as done in [25].

Another effective approach to construct the projection subspace is to employ the Proper Orthogonal Decomposition (POD) algorithm [26]. POD is a method that aims at separating the solution using only time and space, relying on the truncated singular values decomposition of a matrix containing snapshots of the solution; other approaches that lead to separation of time, space, and possibly parameter variables are Reduced Basis (RB), and the Proper Generalized Decomposition (PGD). Both approaches are based on selected specific shape functions. The former uses these to re-discretize the problem [27], whereas the latter defines a suitable residual, which is then minimized by an alternating optimization scheme [28]. The application of Projection-based MOR techniques to non-linear or parametric models introduces additional challenges in achieving a reduced representation. When the model's parameter dependence is affine, the state-space matrices of the ROM can be expressed as a linear combination of smaller matrices, which simplifies the reduction process. However, if the parameter dependence is non-affine and/or the problem is nonlinear, generating the ROM requires recreating the FOM for each variation in the parameters, significantly increasing computational complexity, rendering the approach unsuitable for real-time computing on inexpensive hardware [29]. For parametric problems, the low-order terms of a Taylor series expansion can approximate an affine decomposition of the system matrices. For nonlinear equations, the nonlinear term may be selectively sampled and then interpolated, using approaches such as the Empirical Interpolation Method (EIM) [29], [30].

In the field of thermal modeling, MOR techniques have proven effective in synthesizing accurate thermal networks from numerical models of electronic components, particularly using Krylov-based approaches such as the Multi Point Moment Matching (MPMM) algorithm [21], [22], [22], [23], [31]. These methods have also been extended to manage parametric dependencies and nonlinear thermal conductivity [32], [33], [34]. The main difficulty of handling s2s radiation lies in the expensive calculation of the nonlinear term. Existing techniques for reducing the computational complexity of handling s2s radiation in FEM models have primarily focused on mesh refinement and block partitioning [19], [35], [36]. While these methods help reduce the computational and memory cost of solving and storing the FOM, they are still insufficient for enabling real-time solutions on low-cost hardware, especially for MPC applications.

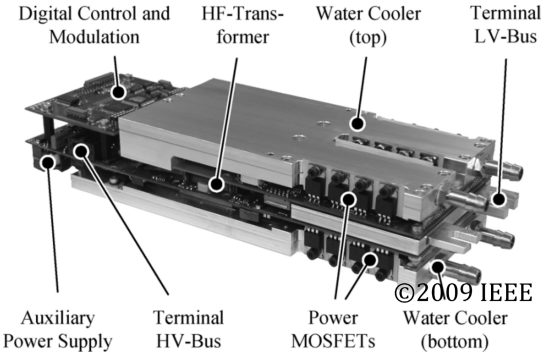

FIGURE 1. High-Current dual active bridge converter for an automotive application [39].

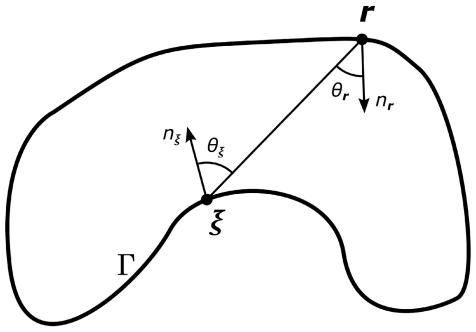

FIGURE 2. Surface-to-surface radiation in an enclosure, adapted from [41].

To tackle this problem, we employ the POD coupled with the Discrete Empirical Interpolation Method (DEIM) [37], which is the discrete version of the EIM. The proposed method is used to construct accurate and computationally light ROMs of PE components, including all radiation effects.

A tailored DEIM approach, designed for the non-local interactions of s2s radiation, is used with interpolation nodes selected through column-pivoted QR factorization [38]. The method is employed to reduce the dimensions of the nonlinear system of equations by combining projection and interpolation, employing snapshots (i.e., temperature maps of the model), to build a basis that is used to project, and thus reduce, the original model.

The POD and DEIM were selected both for their simplicity and effectiveness in producing a ROM. Starting from a time-domain simulation of the FOM, the ROM can be built from an inexpensive truncated SVD of the snapshots, followed by a pivoted QR decomposition. This combination provides a robust framework for efficiently constructing accurate ROMs. Although alternative techniques can be employed to generate a projection basis for the FOM, the primary contribution of this paper lies in the adaptation of the DEIM approach to reduce the nonlinear and non-local term introduced by s2s radiation. The remainder of the paper is structured as follows. First, a summary of surface-to-surface radiation, and its estimation using the radiosity method is presented in Section II. Section III discusses the approach used to reduce the order of the model. After that, in Section IV, the method is employed on a simple DC-DC converter (reported in Fig. 4) to show that even for a simple device, radiation may be relevant, and to prove the effectiveness of the reduction strategy. Finally, the main conclusion of this paper is drawn in Section V.

II. FORMULATION OF THE PROBLEM

A. PROPERTIES OF RADIATIVE SURFACES

When thermal radiation hits a surface it can either be absorbed, reflected, or transmitted. This behavior is described by introducing the absorptivity (α), the reflectivity (ρ), and the transmissivity (τ) coefficients, with sum equal to 1 [40]. For this study we restricted the problem to the case of opaque and diffuse surfaces only, meaning $\tau = 0$ and a uniform rather than specular reflection, a common assumption according to the literature [35], [40], [41]. The reflectivity ρ is written as:

$$\rho = 1 - \alpha. \tag{1}$$

Considering the *total hemispherical* approximation the dependence on temperature and wavelength (λ) of the parameters is averaged out, moreover, by using Kirchhoff's law, ρ can be written in terms of the emissivity ϵ of the surface, since $\epsilon = \alpha$ [40]. The emissivity plays a fundamental role in determining the specific power e emitted from a *blackbody* through to the Stefan-Boltzmann law $e = \epsilon\sigma T_s^4$. The openings of the enclosure are treated as surfaces at ambient temperature that do not reflect incoming radiation, resulting in an equivalent reflectivity equal to zero.

B. CONTINUOUS FORMULATION OF THE RADIOSITY EQUATION

The energy exiting from a point $\mathbf{r}$ lying on an enclosure Γ, called the radiosity $u(\mathbf{r})$, is described by the radiosity equation [41]:

$$u(\mathbf{r}) - \rho(\mathbf{r}) \int_\Gamma u(\xi) G(\mathbf{r}, \xi) V(\mathbf{r}, \xi) d\xi = e(\mathbf{r}), \qquad \mathbf{r}, \xi \in \Gamma, \tag{2}$$

where the second term on the left-hand-side is related to the energy coming from all other points ξ in Γ reflected from r through the reflection coefficient $\rho(\mathbf{r})$. Particularly, the reflected energy depends on the visibility factor $V(\mathbf{r}, \xi) \in [0, 1]$, and $\mathcal{G}(\boldsymbol{r}, \xi)$ defined as:

$$\begin{aligned} \mathcal{G}(\boldsymbol{r}, \xi) &= \frac{(\xi - r) \cdot n_r (\xi - r) \cdot n_\xi}{\pi ||r - \xi||^4} \\ &= \frac{\cos\theta_r \cos\theta_\xi}{\pi ||\boldsymbol{r} - \xi||^2}. \end{aligned} \tag{3}$$

A graphical representation of geometrical quantities of (3) is given in Fig. 2. The right hand side of (2) represents the energy emitted from point $\mathbf{r}$, i.e., $e(\mathbf{r}) = \sigma\epsilon(\mathbf{r})T_r^4$ [42].

C. DISCRETE FORMULATION OF THE RADIOSITY EQUATION

To numerically solve (2), the boundary of the components must be discretized into surface elements, such as triangles. In this paper, to provide a tool that can be seamlessly integrated with FEM software, we decided to use the same FEM mesh of the heat conduction problem. The discrete form factors are obtained by doing the integral average of (3) across each couple of surface patches i, j [41], obtaining:

$$F_{ij} = \frac{1}{A_i} \int_{A_i} \int_{A_j} \frac{\cos\theta_r \cos\theta_\xi}{\pi ||\boldsymbol{r} - \xi||^2} V(\mathbf{r}, \xi) dA_i dA_j. \tag{4}$$

F_{ij} represents the fraction of the radiation leaving the element i that reaches element j, and represents quantitatively *how much two surface elements see each other*. The form factor matrix $\boldsymbol{F} = \{F_{ij}\}$ was calculated by numerically integrating (4) for all $i < j$. The elements in the diagonal are zero, since the surface was discretized with flat triangles, and the other form factors were obtained through the reciprocity relation:

$$A_i F_{ij} = A_j F_{ji}, \tag{5}$$

where A_i represents the area of triangle i [40].

For large models, the form factor computation could be a bottleneck, and the *hemicube algorithm* [43] might provide a more efficient approximation. The visibility factors $V(\boldsymbol{r}, \xi)$, needed in (4) are instead obtained with an implementation of the Ray-Triangle intersection algorithm [44]. The quantity of interest is the net power flowing out of each surface triangle. We now proceed to discretize the radiosity equation (2), obtaining the vector $\boldsymbol{u}$ representing the outwards power of each triangle [36]:

$$(\mathbb{I} - (1 - \epsilon)\boldsymbol{F})\, \boldsymbol{u} = \sigma \epsilon \boldsymbol{T}^4, \tag{6}$$

where ϵ represents the vector of the emissivity values of each triangle, which was used to replace the reflectivity in (2). It should be noted that $\boldsymbol{T}^4$ in this case represents the element-wise fourth power of vector $\boldsymbol{T}$, containing the temperature of each surface element. We can then obtain the net power flowing out of each surface triangle $\boldsymbol{q}_{\text{net}}$. For triangle i, this is the power flowing out from i, minus the sum of the power that flows out of each triangle j which is intercepted by i, and can be represented by the following matrix equation [36]:

$$\boldsymbol{q}_{\text{net}} = (\mathbb{I} - \boldsymbol{F})\, [\mathbb{I} - (1 - \epsilon)\boldsymbol{F}]^{-1}\, \sigma \epsilon \boldsymbol{T}^4 = \boldsymbol{D}\boldsymbol{T}^4. \tag{7}$$

D. COUPLING RADIOSITY WITH THE HEAT CONDUCTION PROBLEM

To construct a model of the device under study, we used the FEM approach applied to the heat conduction equation:

$$\text{In } \Omega: \quad \rho c \frac{\partial T}{\partial t} = \nabla \cdot (k \nabla T) + Q, \tag{8}$$

and coupled with the heat convection equation:

$$\text{On } \partial\Omega: \quad -k \frac{\partial T}{\partial n} = h(T - T_\infty). \tag{9}$$

If thermal radiation is not considered, the FEM model is given by:

$$\boldsymbol{M}\dot{\boldsymbol{x}} + (\boldsymbol{S} + \boldsymbol{H})\boldsymbol{x} = \boldsymbol{q} + \boldsymbol{q}_{\text{conv}}. \tag{10}$$

where $\boldsymbol{M}, \boldsymbol{S} \in \mathbb{R}^{n \times n}$ are the mass and stiffness matrix, and $\boldsymbol{x} \in \mathbb{R}^n$ contains the temperature of each node of the mesh.

In (10), $\boldsymbol{H}$ and $\boldsymbol{q}_{\text{conv}}$ derive from the discretization of the convection boundary condition (9). Furthermore, $\boldsymbol{q}$ represents the internal heat generation of components subject to joule losses.

We now want to couple (10) with (7). The former is a relationship between nodal temperatures $\boldsymbol{x}$ and nodal heat fluxes $\boldsymbol{q} + \boldsymbol{q}_{\text{conv}}$. Instead, equation (7) takes as an input a vector containing the surface elements temperatures $\boldsymbol{T}$, and returns $\boldsymbol{q}_{\text{net}}$, i.e., the net heat flux due to radiation on each surface element. To couple surface-to-surface radiation with (10), we need to express it as a function of the nodal temperature, and the net heat flux should be mapped into nodes instead of surface elements. Matrix $\boldsymbol{N}$ is defined as the operator performing the average of the nodal temperatures, yielding the temperature of each triangle. The net radiation on each element is mapped on the nodes through matrix $\boldsymbol{B} = \{B_{li}\} = \int_{\Gamma_i} \phi_l d\Gamma_i$, where ϕ_l is the basis function of node l [42]. We can now express the radiation contribution in each mesh node using:

$$\boldsymbol{q}_{\text{rad}} = \boldsymbol{B}\boldsymbol{D}\boldsymbol{T}^4 = \boldsymbol{G}\boldsymbol{T}^4. \tag{11}$$

Combining the radiation boundary condition (11) with the original system of equations (10) returns the following system of nonlinear equations:

$$\boldsymbol{M}\dot{\boldsymbol{x}} + (\boldsymbol{S} + \boldsymbol{H})\boldsymbol{x} = \boldsymbol{q} + \boldsymbol{q}_{\text{conv}} + \boldsymbol{G}\,(\boldsymbol{N}\boldsymbol{x})^4\,. \tag{12}$$

E. SOLVING THE TIME-DEPENDENT PROBLEM

The FEM is described by local relationships between quantities, in particular, the temperature in a node of the mesh depends on the temperature of nearby ones. This provides a large, but sparse system of equations that describes the problem. Instead, the surface-to-surface radiation boundary condition defines a non-local coupling between all surface nodes. This makes matrix $\boldsymbol{G}$ dense, thus significantly increasing the computational burden. Dense matrix operations, combined with the fact that (12) is nonlinear in $\boldsymbol{x}$ make the problem expensive to solve, especially for time domain simulations.

One possibility is to solve for $\boldsymbol{x}$ the nonlinear problem (12) at each time step of the problem, but to reduce the computation time, we chose an approximate approach. Without considering the effect of thermal radiation, we discretized the resulting system using the Backward Euler Algorithm [45], approximating the solution at each step via:

$$\boldsymbol{x}_{k+1} \approx \boldsymbol{x}_k + \Delta t \boldsymbol{f}(\boldsymbol{x}_{k+1}, t_{k+1}), \tag{13}$$

where Δt is the time-step and $\boldsymbol{f}$ is obtained from (12) by algebraic manipulations.

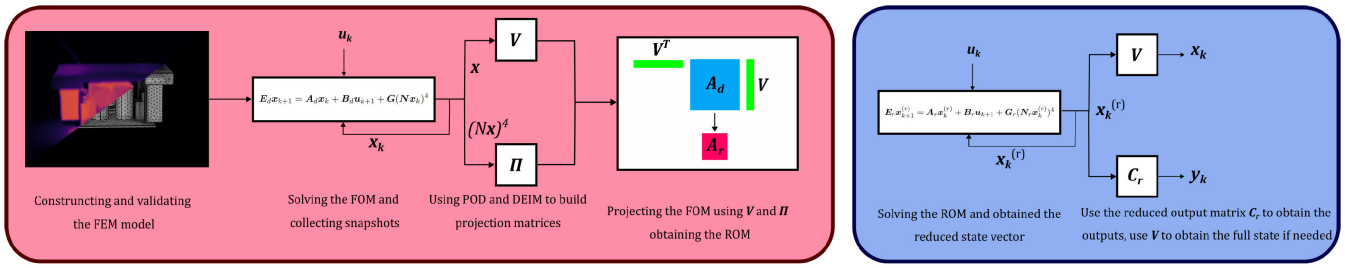

FIGURE 3. MOR process: Elements in the red rectangle need to be performed only once in the offline phase. The blue rectangle represents obtaining new outputs in the online phase.

The volumetric heat generation $\boldsymbol{q}$ and the convection boundary condition $\boldsymbol{q}_{\text{conv}}$, have been replaced with the product of an input matrix $\boldsymbol{P}$ times the input $\boldsymbol{u}$. Both the state vector and the input are functions of time.

Performing these operations, returned the following relationship:

$$\boldsymbol{E}_d\boldsymbol{x}_{k+1} = \boldsymbol{A}_d\boldsymbol{x}_k + \boldsymbol{B}_d\boldsymbol{u}_{k+1}, \tag{14}$$

where:

$$\boldsymbol{E}_d = \boldsymbol{M} + \Delta t(\boldsymbol{S} + \boldsymbol{H}) \tag{15}$$
$$\boldsymbol{A}_d = \boldsymbol{M} \tag{16}$$
$$\boldsymbol{B}_d = \Delta t\boldsymbol{P}. \tag{17}$$

Discretizing (12) using the Backward Euler method would require moving the nonlinear $\boldsymbol{G}(\boldsymbol{N}\boldsymbol{x})^4$ term to the left-hand side of (14), requiring the use of a nonlinear solver at each time step. For this reason, considering the slow evolution of the temperature w.r.t. the chosen time step, we opted for an approximated solution. The nonlinear term was calculated using the temperature distribution from the previous time step, obtaining the following equation:

$$\boldsymbol{E}_d\boldsymbol{x}_{k+1} = \boldsymbol{A}_d\boldsymbol{x}_k + \boldsymbol{B}_d\boldsymbol{u}_{k+1} + \boldsymbol{G}(\boldsymbol{N}\boldsymbol{x}_k)^4. \tag{18}$$

This approach was compared with the more accurate one (i.e., by actually solving the non-linear problem at each time step) on smaller problems but with similar dynamics. With the chosen time step, the two methods are comparable (i.e., discrepancies below 0.1 % were obtained).

III. MODEL ORDER REDUCTION

To reduce the cost of simulating (18) which is a high dimensional model, we look for a surrogate model with a much lower state dimension $r \ll n$. This is obtained using the POD, combined with the DEIM [37] to handle the nonlinearity of the system. More precisely, we perform the following steps, presented also in Fig. 3:

1) We run the FOM for s different combinations of inputs $\boldsymbol{u}$ and initial states. We collect the snapshot matrix $\tilde{\boldsymbol{V}} \in \mathbb{R}^{n\times n_T s}$ containing the solution of the FOM for all inputs and for each n_T timesteps. Analogously, we store the matrix $\tilde{\boldsymbol{W}} \in \mathbb{R}^{n_E\times n_T s}$ containing the quantities $(\boldsymbol{N}\boldsymbol{x}_k)^4$ where n_E is the number of elements in the finite element mesh.
2) We extract matrices $\boldsymbol{V}, \boldsymbol{W}$ with r and r_{DEIM} orthogonal columns spanning low-dimensional subspaces approximating the ranges of $\tilde{\boldsymbol{V}}, \tilde{\boldsymbol{W}}$, respectively. This can be either done with a truncated SVD for moderate n, or with a randomized rangefinder for larger problems [46]; the latter only requires matrix-vector multiplications of $\tilde{\boldsymbol{V}}$ and $\tilde{\boldsymbol{W}}$ with $\mathcal{O}(r + r_{\text{DEIM}})$ random vectors.

To obtain the reduced model, we approximate $\boldsymbol{x}(t) \approx \boldsymbol{V}\boldsymbol{x}^{(r)}(t)$ and impose a Galerkin condition, which yields the $r \times r$ nonlinear system; we discretize it by Backward Euler as we did for the FOM, obtaining:

$$\boldsymbol{E}_r\boldsymbol{x}_{k+1}^{(r)} = \boldsymbol{A}_r\boldsymbol{x}_k^{(r)} + \boldsymbol{B}_r\boldsymbol{u}_{k+1} + \boldsymbol{V}^T\boldsymbol{G}(\boldsymbol{N}\boldsymbol{V}\boldsymbol{x}_k^{(r)})^4, \tag{19}$$

where:

$$\boldsymbol{E}_r = \boldsymbol{V}^T\boldsymbol{E}_d\boldsymbol{V}, \quad \boldsymbol{A}_r = \boldsymbol{V}^T\boldsymbol{A}_d\boldsymbol{V}, \ \boldsymbol{B}_r = \boldsymbol{V}^T\boldsymbol{B}_d.$$

Evaluating the nonlinear term $\boldsymbol{V}^T\boldsymbol{G}(\boldsymbol{N}\boldsymbol{V}\boldsymbol{x}_k^{(r)})^4$ would require assembling the full order solution. Hence, we further approximate it with a DEIM approach as:

$$(\boldsymbol{N}\boldsymbol{V}\boldsymbol{x}_k^{(r)})^4 \approx \boldsymbol{W}\boldsymbol{y}_k, \quad \boldsymbol{y}_k := (\mathcal{I}^T\boldsymbol{W})^{-1}\left[\mathcal{I}^T(\boldsymbol{N}\boldsymbol{V}\boldsymbol{x}_k^{(r)})^4\right],$$

where $\mathcal{I}$ is a $n_E \times r_{\text{DEIM}}$ is a row-selection matrix (i.e, it contains r_{DEIM} columns of the $n_E \times n_E$ identity matrix). These columns can be chosen with well-established techniques that guarantee the invertibility of $\mathcal{I}^T\boldsymbol{W}$; we use the one based on the pivoted QR decomposition proposed in [38]. Note that in view of the component-wise nature of the nonlinearity, we have $\mathcal{I}^T(\boldsymbol{N}\boldsymbol{V}\boldsymbol{x}_k^{(r)})^4 = (\mathcal{I}^T\boldsymbol{N}\boldsymbol{V}\boldsymbol{x}_k^{(r)})^4$. Substituting this approximation in (19) yields:

$$\boldsymbol{E}_r\boldsymbol{x}_{k+1}^{(r)} = \boldsymbol{A}_r\boldsymbol{x}_k^{(r)} + \boldsymbol{B}_r\boldsymbol{u}_{k+1} + \boldsymbol{G}_r(\boldsymbol{N}_r\boldsymbol{x}_k^{(r)})^4,$$

where the matrices:

$$\boldsymbol{G}_r := \boldsymbol{V}^T\boldsymbol{G}\boldsymbol{W}(\mathcal{I}^T\boldsymbol{W})^{-1} \in \mathbb{R}^{r\times r_{\text{DEIM}}},$$
$$\boldsymbol{N}_r := \mathcal{I}^T\boldsymbol{N}\boldsymbol{V} \in \mathbb{R}^{r_{\text{DEIM}}\times r}$$

can be computed once and for all in the offline phase. The reduced model is integrated with the same Backward Euler scheme with explicit nonlinearity used for the FOM. In this

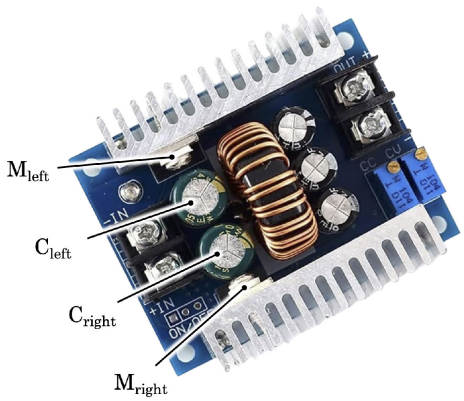

FIGURE 4. Picture of the DC-DC converter with marked regions of interest.

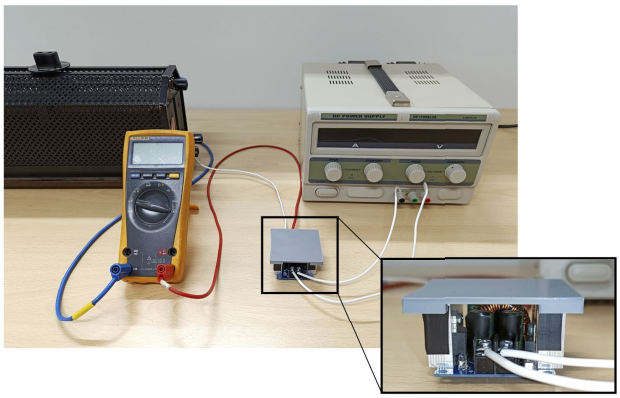

FIGURE 5. Experimental setup.

framework, computing each step of the ROM costs $\mathcal{O}(r(r + r_{\text{DEIM}}))$ flops, assuming that a Cholesky factorization of E_r is precomputed in the offline phase.

IV. NUMERICAL EXPERIMENTS

A. PRELIMINARY ANALYSIS

The proposed approach is applied to a simple DC-DC converter (reported in Fig. 4) to show that even for a simple device, radiation is relevant, and to prove the effectiveness of the reduction strategy.

The DC-DC converter has been modeled using the Finite Element Analysis (FEA) software COMSOL Multiphysics®. The step-down converter used can operate with an input voltage between $6-40$V and an output voltage of $1.5-30$V, the device is covered with a plastic lid to resemble an enclosure. The input was connected to a DC power supply and the output to a variable resistor. The setup used for the experiments can be seen in Fig. 5. Thermal pictures were taken with a Flir T420 thermal camera, and capacitors and heat sinks were covered with black electrical tape to provide the same value of surface emissivity. Fig. 6a was taken with the module in steady-state operating at the conditions seen in Table 1. The unknown parameters of the numerical model were fit using temperature measurements taken with the thermal camera and the results were compared to the original as seen in Fig. 6b.

TABLE 1. Operating conditions of the power converter.

V_{in}	I_{in}	V_{out}	I_{out}
38.97V	2.97A	14.75V	7.21A

TABLE 2. Comparison between steady-state measurements and simulation of capacitors and MOSFETs surface temperatures °C.

	M_{left}	C_{left}	C_{right}	M_{right}
measurement	98.7	84.5	78.7	68.6
s2s+s2a	100.8	84.6	75.2	68.4
without radiation	112.6	98.7	85.2	73.5
only s2a	92.8	70.5	62.3	62.4

The FEA model is a simplification of the real device, considering heat generation in the components subject to losses, and heat conduction with radiation and convection boundary conditions. By disabling the surface-to-surface and surface-to-ambient boundary conditions, we can see in Fig. 6c that the temperature readings differ substantially from the ones obtained with the more accurate model. It should be noted that the thermal maps are presented all with the same scale of Fig. 6c for ease of comparison. This simple demonstration still shows that the effect of surface-to-surface radiation is significant even for this simple component. This can be verified quantitatively in Table 2, where the measurements from the thermal camera are compared with the surface averaged temperatures in locations of interest, i.e., capacitors and MOSFETs shown in Fig. 4. Table 2 shows the impact of modeling surface-to-surface radiation on the average temperature of passive components. The temperature of the capacitors is greatly affected by the proximity of the coil and the MOSFETs, consequently, they change significantly if the s2s boundary condition is removed.

B. MODEL ORDER REDUCTION

The FEM model of the converter described in Section IV-A, was then constructed by using proprietary numerical tools developed in the MATLAB® environment. The resulting system has one input corresponding to the total dissipated power, which is then distributed in the heat-generating regions of the device. The outputs represent the average temperatures in volumes of interest of the device. The matrices needed for radiosity were built as explained in previous sections. In Fig. 7, the average temperature of the left capacitor (C_{left} in Fig. 4) subject to the input power shown in Fig. 9 is depicted. Analogously, Fig. 8 shows the temperature evolution of the MOSFET (averaged temperature). The model is first simulated without radiation, then with both s2s and s2a, and finally by applying only the s2a boundary condition, considering the total visibility of the ambient for each radiating surface. Fig. 7 and Fig. 8 emphasize the different trajectories taken by the temperature, further validating the impact of considering s2s radiation for this device.

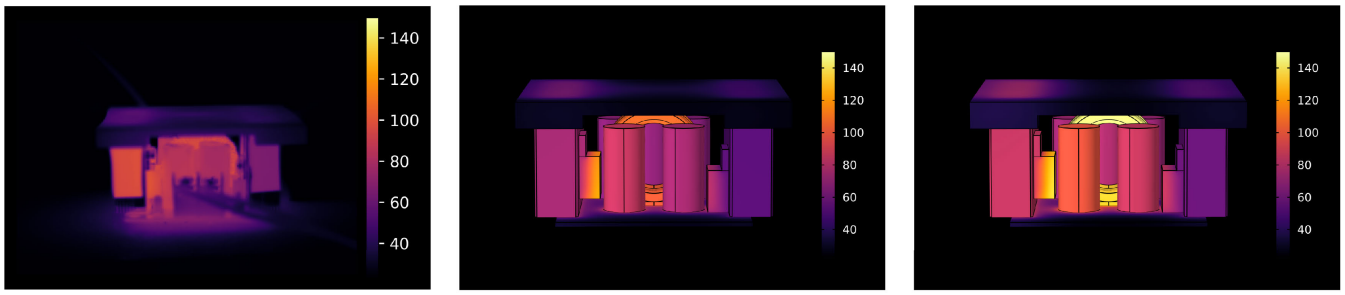

(a) Thermal image of the device under load (b) FEA simulation considering thermal radiation (c) FEA simulation ignoring thermal radiation

FIGURE 6. Comparison between measurements and FEA simulations. Color bar in °C.

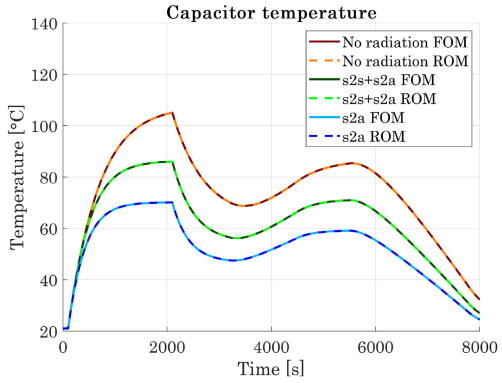

FIGURE 7. Temperature estimate in the left capacitor with and without the contribution of thermal radiation.

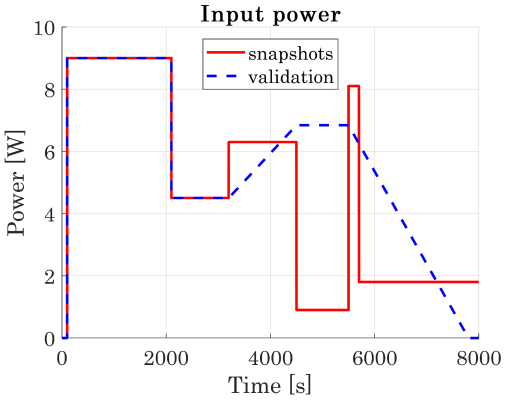

FIGURE 9. Input power during snapshots collection and ROM validation.

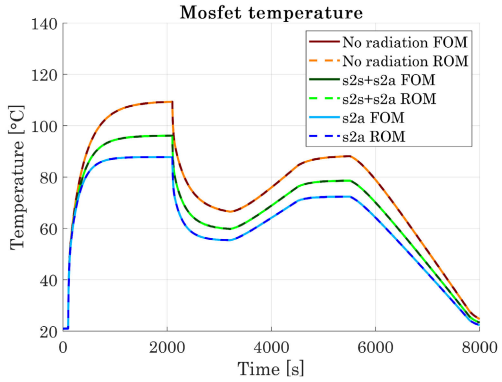

FIGURE 8. Temperature estimate in the left MOSFET with and without the contribution of thermal radiation.

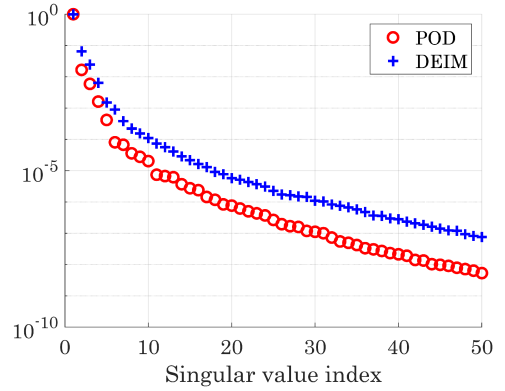

FIGURE 10. Normalized singular value decay of the first 50 singular values of the POD and DEIM snapshot matrices.

To perform the MOR, snapshots must be computed, so the FOM was run using the series of steps of input powers shown in Fig. 9 with a time step of 1 second. Once the snapshots are collected, selecting the number of singular vectors for the POD and DEIM involves balancing model size and accuracy. The decay of singular values in the snapshot matrices provides an initial indication of the approach's effectiveness. A sharp decline suggests that a small number of modes can capture most of the information in the dataset. As shown in Fig. 9, both the POD and DEIM snapshots exhibit a significant drop in the first few singular values.

The singular value decay of the snapshot matrices provides information about the reconstruction error of the snapshots, but not about the ROM solution error [29]. The ROM error was derived by testing it on new input data shown in Fig. 9 using different numbers of POD and DEIM modes. As presented in Fig. 11, the model improvement becomes less and less significant as the number of modes increases.

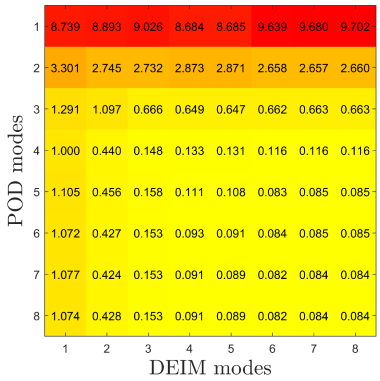

FIGURE 11. Root mean squared error between FOM and ROM temperature prediction in the left mosfet as a function of the number of POD and DEIM modes considered.

TABLE 3. Computation time and memory requirements comparison between full and reduced order model.

	n	s_G	Memory	ct
FOM	23619	23619×29515	5332 MB	1h 52min
ROM	7	7×6	3.23 kB	$0.61s$

TABLE 4. Root Mean Squared Error (RMSE) between ROM and FOM temperature predictions.

	M_{left}	C_{left}	C_{right}	M_{right}
RMSE	0.0822	0.0458	0.0339	0.0471

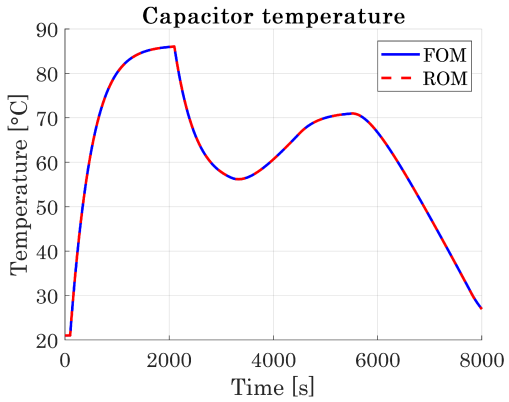

FIGURE 12. Left capacitor temperature during validation.

Although using just three POD and DEIM modes provides satisfactory results, the final ROM was built using 7 POD and 6 DEIM modes to obtain a more accurate ROM. As reported in Table 3, the number of states n was reduced from 23619 to 7. The size s_G of the radiation matrix $\boldsymbol{G}$ in (11) was reduced from 23619×29515 to 7×6. The computation time needed to run the simulation was reduced from 1 hr 52 min to less than 1 second, and the memory used to store the matrices was reduced from 5332 MB to less than 4 kB.

The resulting model operates faster than real-time, making it suitable for MPC applications, and incorporating s2s and s2a radiation leads to a manageable 22% increase in computation time compared to the linear ROM. As presented in Fig.12, the temperature estimates from the ROM closely align with those predicted by the FOM in both the low and high temperature regions, where the effects of radiation are more pronounced. Moreover, temperature curves in Fig. 7 and Fig. 8 demonstrate the accuracy of the reduction method applied to both the linear model and the model that includes only s2a radiation.

The ROM results were compared with those from the FOM to assess any loss of accuracy. As shown in Table 4, the ROM accurately predicts the temperature increase in the components of interest, confirming the validity of the approach.

V. CONCLUSION

A Proper Orthogonal Decomposition (POD) coupled with the Discrete Empirical Interpolation Method (DEIM) approach has been applied to reduce the computational complexity of the heat conduction problem coupled with the surface-to-ambient and surface-to-surface radiation boundary conditions [36], [38]. The same mesh used for the heat conduction discretization is adopted to build the matrices needed for surface-to-ambient and surface-to-surface radiation, and the resulting model is then reduced. Thanks to the POD-DEIM method, high-fidelity physics-based models, can be seamlessly transformed into accurate Reduced Order Models (ROMs). By using this technique, both the computation time and memory needed to store the model of the device are greatly reduced, while the prediction error of the reduced order model is negligible. Finally, further improvements can be also achieved by employing faster strategies to build the radiosity matrix, in particular the calculation of the visibility factor, the main bottleneck of the proposed method. More efficient techniques can also take advantage of programmable graphics hardware to accelerate computations [43]. Starting from the proposed tool, future research will focus on machine-learning approaches to further decrease the complexity of deriving the reduced order model.

REFERENCES

[1] A. Stippich, C. H. Van Der Broeck, A. Sewergin, A. H. Wienhausen, M. Neubert, P. Schülting, S. Taraborrelli, H. van Hoek, and R. W. De Doncker, "Key components of modular propulsion systems for next generation electric vehicles," *CPSS Trans. Power Electron. Appl.*, vol. 2, no. 4, pp. 249–258, Dec. 2017.

[2] S. Yano, Y. Nakayama, H. Kobayashi, S. Hiramatsu, M. Yoshida, K. Onda, K. Hayashi, and K. Yamazaki, "Development of compact power control unit for HEVs," in *Proc. IEEE Energy Convers. Congr. Expo. (ECCE)*, Oct. 2017, pp. 584–588.

[3] E. Laloya, Ó. Lucía, H. Sarnago, and J. M. Burdío, "Heat management in power converters: From state of the art to future ultrahigh efficiency systems," *IEEE Trans. Power Electron.*, vol. 31, no. 11, pp. 7896–7908, Nov. 2016.

[4] S. Jones-Jackson, R. Rodriguez, Y. Yang, L. Lopera, and A. Emadi, "Overview of current thermal management of automotive power electronics for traction purposes and future directions," *IEEE Trans. Transport. Electrific.*, vol. 8, no. 2, pp. 2412–2428, Jun. 2022.

[5] L. Han, L. Liang, Y. Kang, and Y. Qiu, "A review of SiC IGBT: Models, fabrications, characteristics, and applications," *IEEE Trans. Power Electron.*, vol. 36, no. 2, pp. 2080–2093, Feb. 2021.

[6] A. Bindra, "Wide-bandgap-based power devices: Reshaping the power electronics landscape," *IEEE Power Electron. Mag.*, vol. 2, no. 1, pp. 42–47, Mar. 2015.
[7] G. Iannaccone, C. Sbrana, I. Morelli, and S. Strangio, "Power electronics based on wide-bandgap semiconductors: Opportunities and challenges," *IEEE Access*, vol. 9, pp. 139446–139456, 2021.
[8] S. Anandan and V. Ramalingam, "Thermal management of electronics: A review of literature," *Thermal Sci.*, vol. 12, no. 2, pp. 5–26, 2008.
[9] S. Vazquez, J. Rodriguez, M. Rivera, L. G. Franquelo, and M. Norambuena, "Model predictive control for power converters and drives: Advances and trends," *IEEE Trans. Ind. Electron.*, vol. 64, no. 2, pp. 935–947, Feb. 2017.
[10] N. Baker, M. Liserre, L. Dupont, and Y. Avenas, "Improved reliability of power modules: A review of online junction temperature measurement methods," *IEEE Ind. Electron. Mag.*, vol. 8, no. 3, pp. 17–27, Sep. 2014.
[11] M. Musallam and C. Mark Johnson, "Real-time compact thermal models for health management of power electronics," *IEEE Trans. Power Electron.*, vol. 25, no. 6, pp. 1416–1425, Jun. 2010.
[12] C. H. van der Broeck, R. D. Lorenz, and R. W. De Doncker, "Monitoring 3-D temperature distributions and device losses in power electronic modules," *IEEE Trans. Power Electron.*, vol. 34, no. 8, pp. 7983–7995, Aug. 2019.
[13] F. Fan Wang, "Electronics packaging simplified radiation heat transfer analysis method," in *Proc. 9th Intersoc. Conf. Thermal Thermomech. Phenomena Electron. Syst.*, vol. 1, Jun. 2004, pp. 613–617.
[14] E. Dallago and G. Venchi, "Thermal characterization of compact electronic systems: A portable PC as a study case," *IEEE Trans. Power Electron.*, vol. 17, no. 2, pp. 187–195, Mar. 2002.
[15] E. Papanicolaou and S. Gopalakrishna, "Natural convection in shallow, horizontal air layers encountered in electronic cooling," *J. Electron. Packag.*, vol. 117, no. 4, pp. 307–316, Dec. 1995.
[16] R. Siegel, *Thermal Radiation Heat Transfer: Vol. 3: Radiation Transfer With Absorbing, Emitting, and Scattering Media*, vol. 164. Washington, DC, USA: Scientific and Technical Information Division, National Aeronautics and Space Administration, 1971.
[17] V. d'Alessandro and N. Rinaldi, "A critical review of thermal models for electro-thermal simulation," *Solid-State Electron.*, vol. 46, no. 4, pp. 487–496, Apr. 2002.
[18] J. R. Gosselin and Q. Chen, "A computational method for calculating heat transfer and airflow through a dual-airflow window," *Energy Buildings*, vol. 40, no. 4, pp. 452–458, Jan. 2008.
[19] N. Qatanani and I. Alzeer, "On the fast matrix computation for the heat radiation integral equation," *Int. J. Math. Comput. Sci.*, vol. 1, no. 4, pp. 461–472, Jun. 2006.
[20] P. Benner et al., *Model Order Reduction. System- and Data-Driven Methods and Algorithms* (Model Order Reduction), vol. 1. Berlin, Germany: De Gruyter, 2021.
[21] L. Codecasa, V. d'Alessandro, A. Magnani, N. Rinaldi, and P. J. Zampardi, "Fast novel thermal analysis simulation tool for integrated circuits (FANTASTIC)," in *Proc. 20th Int. Workshop Thermal Investigations ICs Syst.*, Sep. 2014, pp. 1–6.
[22] L. Codecasa, D. D'Amore, and P. Maffezzoni, "Compact thermal networks for modeling packages," *IEEE Trans. Compon. Packag. Technol.*, vol. 27, no. 1, pp. 96–103, Mar. 2004.
[23] L. Codecasa, D. D'Amore, and P. Maffezzoni, "An Arnoldi based thermal network reduction method for electro-thermal analysis," *IEEE Trans. Compon. Packag. Technol.*, vol. 26, no. 1, pp. 186–192, Mar. 2003.
[24] V. Simoncini, "Computational methods for linear matrix equations," *SIAM Rev.*, vol. 58, no. 3, pp. 377–441, Jan. 2016.
[25] G. Floros, N. Evmorfopoulos, and G. Stamoulis, "Efficient IC hotspot thermal analysis via low-rank model order reduction," *Integration*, vol. 66, pp. 1–8, May 2019.
[26] A. Chatterjee, "An introduction to the proper orthogonal decomposition," *Current Sci.*, vol. 78, no. 7, pp. 808–817, Jan. 2000.
[27] B. Haasdonk, "Reduced basis methods for parametrized PDEs—A tutorial introduction for stationary and instationary problems," in *Model Reduction and Approximation*, P. Benner, M. Ohlberger, A. Cohen, and K. Willcox, Eds., Philadelphia, PA, USA: SIAM, 2017, ch. 2, pp. 65–136.
[28] F. Chinesta, P. Ladeveze, and E. Cueto, "A short review on model order reduction based on proper generalized decomposition," *Arch. Comput. Methods Eng.*, vol. 18, no. 4, pp. 395–404, Nov. 2011.
[29] P. Benner, S. Gugercin, and K. Willcox, "A survey of projection-based model reduction methods for parametric dynamical systems," *SIAM Rev.*, vol. 57, no. 4, pp. 483–531, Jan. 2015.
[30] M. Barrault, Y. Maday, N. C. Nguyen, and A. T. Patera, "An 'empirical interpolation' method: Application to efficient reduced-basis discretization of partial differential equations," *Comp. Rendus. Mathématique*, vol. 339, no. 9, pp. 667–672, Oct. 2004.
[31] L. Codecasa, D. D'Amore, and P. Maffezzoni, "Compact modeling of electrical devices for electrothermal analysis," *IEEE Trans. Circuits Syst. I: Fundam. Theory Appl.*, vol. 50, no. 4, pp. 465–476, Apr. 2003.
[32] D. Celo, X. Guo, P. K. Gunupudi, R. Khazaka, D. J. Walkey, T. Smy, and M. S. Nakhla, "The creation of compact thermal models of electronic components using model reduction," *IEEE Trans. Adv. Packag.*, vol. 28, no. 2, pp. 240–251, May 2005.
[33] L. Codecasa, V. d'Alessandro, A. Magnani, and A. Irace, "Circuit-based electrothermal simulation of power devices by an ultrafast nonlinear MOR approach," *IEEE Trans. Power Electron.*, vol. 31, no. 8, pp. 5906–5916, Aug. 2016.
[34] L. Codecasa, V. d'Alessandro, A. Magnani, and N. Rinaldi, "Compact dynamic modeling for fast simulation of nonlinear heat conduction in ultra-thin chip stacking technology," *IEEE Trans. Compon., Packag., Manuf. Technol.*, vol. 4, no. 11, pp. 1785–1795, Nov. 2014.
[35] C. Scheiblich, V. Kolitsas, and W. M. Rucker, "Compression of the radiative heat transfer BEM matrix of an inductive heating system using a block-oriented wavelet transform," *IEEE Trans. Magn.*, vol. 45, no. 3, pp. 1712–1715, Mar. 2009.
[36] A. Voigt and C. Weichmann, "Adaptive FEM/BEM coupling for solving global heat transfer in high-temperature furnaces," *Numer. Heat Transf., B, Fundam.*, vol. 51, no. 1, pp. 25–41, Jan. 2007.
[37] S. Chaturantabut and D. C. Sorensen, "Nonlinear model reduction via discrete empirical interpolation," *SIAM J. Sci. Comput.*, vol. 32, no. 5, pp. 2737–2764, Jan. 2010.
[38] Z. Drmač and S. Gugercin, "A new selection operator for the discrete empirical interpolation method–improved a priori error bound and extensions," *SIAM J. Sci. Comput.*, vol. 38, no. 2, pp. A631–A648, Jan. 2016.
[39] F. Krismer and J. W. Kolar, "Accurate power loss model derivation of a high-current dual active bridge converter for an automotive application," *IEEE Trans. Ind. Electron.*, vol. 57, no. 3, pp. 881–891, Mar. 2010.
[40] T. L. Bergman, F. P. Incropera, A. S. Lavine, and D. P. Dewitt, *Fundamentals of Heat and Mass Transfer*, 7th ed., Hoboken, NJ, USA: Wiley, 2011.
[41] A. Voigt, N. Hanssen, and C. Weichmann, "The radiosity equation for solving global heat transfer in industrial furnaces," *Math. Comput. Model.*, vol. 39, nos. 2–3, pp. 145–150, Jan. 2004.
[42] C. Weichmann, R. Backofen, and A. Voigt, "Time dependent 3D heat radiation calculation in high temperature furnaces," *WIT Trans. Eng. Sci.*, vol. 46, pp. 1–10, Jan. 2004.
[43] S. Kramer, R. Gritzki, A. Perschk, M. Rösler, and C. Felsmann, "Numerical simulation of radiative heat transfer in indoor environments on programmable graphics hardware," *Int. J. Thermal Sci.*, vol. 96, pp. 345–354, Oct. 2015.
[44] T. Möller and B. Trumbore, "Fast, minimum storage ray-triangle intersection," *J. Graph. Tools*, vol. 2, no. 1, pp. 21–28, Jan. 1997.
[45] C. Vuik, F. J. Vermolen, M. B. Van Gijzen, and M. J. Vuik, "Numerical methods for ordinary differential equations," TU Delft Open, 2023, doi: 10.5074/T.2023.001.
[46] N. Halko, P. G. Martinsson, and J. A. Tropp, "Finding structure with randomness: Probabilistic algorithms for constructing approximate matrix decompositions," *SIAM Rev.*, vol. 53, no. 2, pp. 217–288, Jan. 2011.

MATTEO ZORZETTO was born in Mirano, Italy, in 1999. He received the M.S. degree in electrical engineering from Università degli Studi di Padova, Padua, Italy, in 2023, where he is currently pursuing the degree in electrical engineering. His research interests include model order reduction, model predictive control, surrogate modeling, optimization, and the enhancement of these methods using data-driven techniques, with a focus on electromagnetic devices.

RICCARDO TORCHIO was born in Padua, Italy, in 1992. He received the M.S. degree in electrical engineering from Università degli Studi di Padova, Padua, in 2016, and the Ph.D. degree in electrical engineering from Università degli Studi di Padova and the Grenoble Electrical Engineering Laboratory (G2ELab), Université Grenoble Alpes, Grenoble, France, in December 2019. He is currently an Assistant Professor (RTDa) with Università degli Studi di Padova. His research interests include numerical methods, optimizations, low-rank compression techniques, uncertainty quantifications, wireless power transfer applications, model order reduction, model predictive control, and the development of integral formulations for the study of low- and high-frequency electromagnetic devices.

FRANCESCO LUCCHINI received the M.S. degree in mathematical engineering from Università degli Studi di Padova, Padua, Italy, in 2019, and the Ph.D. degree in fusion science and engineering from Università degli Studi di Padova and the University of Ghent, Ghent, Belgium, in March 2023. He is currently an Assistant Professor (RTDa) with Università degli Studi di Padova. His research interests include numerical methods, optimizations, the development of integral formulations for the study of electromagnetic devices, and the modeling of gas-insulated high-voltage components for neutral beam injectors.

STEFANO MASSEI was born in Livorno, Italy, in 1988. He received the M.S. degree in mathematics from the University of Pisa, Pisa, in 2013, and the Ph.D. degree in mathematics from Scuola Normale Superiore, Italy, in March 2017. He is currently an Assistant Professor (RTDb) with the University of Pisa. His research interests include numerical linear algebra, low-rank approximation, optimization, scientific computing, model order reduction, and numerical methods for Markov chain models.

LEONARDO ROBOL received the M.S. degree in mathematics from the University of Pisa, Pisa, in 2012, and the Ph.D. degree in mathematics from Scuola Normale Superiore, Pisa, in 2015. From 2015 to 2017, he was a Postdoctoral Fellow at with the Department of Computer Science, KU Leuven, Belgium. From 2017 to 2018, he was a Researcher at the Institute of Information Science and Technologies "Alessandro Faedo," CNR. Since 2018, he has been an Assistant Professor with the Department of Mathematics, University of Pisa. His research interests include low-rank approximation, matrix functions and matrix equations, linear and nonlinear structured eigenvalue problems, tensor equations, Markov chains, and structural mechanics.

FABRIZIO DUGHIERO is a Full Professor of electromagnetic processing of materials (EPM) with Università degli Studi di Padova, Padua, Italy, and the Chief Scientist with the Laboratory of Electroheat, Università degli Studi di Padova. He has been the Founder of a spin-off company (InovaLab) and Unismart Padua Enterprise Ltd., Padua, a new in-house company aimed to develop Technology and Knowledge Transfer of Università degli Studi di Padova. He is currently the Director of the Department of Industrial Engineering, Università degli Studi di Padova. His current research activity, documented by more than 180 scientific publications, mainly deals with theoretical aspects and applications of EPM and electroheat technologies.

Open Access funding provided by 'Università degli Studi di Padova' within the CRUI CARE Agreement